Supplementary Online Material

Assumptions

- The lipid bilayer is a modeled as a thin elastic shell. We use the Helfrich energy [1] based on the assumption that the thickness of the bilayer is negligible compared to its radius of curvature. This allows us to neglect shear deformations and consider classical Kirchoff-Love shell kinematics for thin shell geometries. Furthermore, we assume that the membrane is areally incompressible since the maximum elastic stretch is only 4 $\%$ [2]. This incompressibility constraint is numerically enforced using a Lagrange multiplier field. Additionally, we ignore any fluid [3] and friction [4] properties of the bilayer. Thus, the membrane is in mechanical equilibrium at all times.

- The lack of resistance to shear deformation modes in the Helfrich energy formulation can result in rigid body (zero energy) modes of deformation. To circumvent this limitation, in the 3D numerical simulations, we add shear stabilization terms to the classical Helfrich energy functional [5]. These stabilization terms are of a smaller magnitude relative to the traditional bending energy terms, and restore stability to the numerical model without significantly effecting the kinematics of bending.

- The membrane tubule is modeled both as an axisymmetric and 3D lipid bilayer. A pinching force is applied at different locations - 'cap', 'tube', and 'base' (Fig. 2). Since the tether is pulled from a membrane reservoir that can buffer changes in membrane tension [6, 7], we assume that elastic properties like membrane tension and bending rigidity are constant.

- Since we do not consider the fluid properties of the membrane, we cannot consider scission explicitly. We assume that the large stresses at the neck can lead to the formation of a hemi-fission intermediate [8, 9].

- The interaction of the constriction proteins and the membrane tubule can be numerically thought of as a contact model where the proteins apply a contact force of constriction on the tubule. Here, we do not consider a contact model but rather apply a follower load type collar pressure in the constriction region.

Thin shell formulations: Axisymmetric and 3D models

Equilibrium equations for the axisymmetric model

First, we write the force balance on the membrane as

$$\nabla \cdot \boldsymbol{\sigma} + p\mathbf{n} = \mathbf{f}, \tag{1}$$

where $\boldsymbol{\sigma}$ is the stress tensor, p is the pressure difference between the inside and outside of the volume bounded by the membrane, and $\mathbf{f}$ is any externally applied force per unit area on the membrane. In our simulations, we assume that the tubule has equilibrated the pressure difference, and thus set p to 0. $\mathbf{f}$ includes both the axial and pinching forces applied on the membrane. By introducing the covariant derivative as $()_{;\alpha}$, the surface divergence in Eq. 1 can be rewritten as [10]

$$\nabla \cdot \boldsymbol{\sigma} = \boldsymbol{\sigma}^{\alpha}_{;\alpha} = (\sqrt{a})^{-1}(\sqrt{a}\boldsymbol{\sigma}^{\alpha})_{,\alpha}, \tag{2}$$

where a is the determinant of the first fundamental form metric $a_{\alpha\beta}$. The surface stresses in Eq. 1 can be split into normal and tangential component given by

$$\boldsymbol{\sigma}^{\alpha} = \boldsymbol{T}^{\alpha} + S^{\alpha}\mathbf{n}, \tag{3}$$

where

$$\mathbf{T}^{\alpha} = T^{\alpha\beta}\mathbf{a}_{\beta}, \qquad T^{\alpha\beta} = \sigma^{\alpha\beta} + b^{\beta}_{\mu}M^{\mu\alpha}, \qquad S^{\alpha} = -M^{\alpha\beta}_{;\beta}. \tag{4}$$

The two tensors $\sigma^{\alpha\beta}$ and $M^{\alpha\beta}$ can be expressed by the derivative of F, the energy per unit mass, with respect to the coefficients of the first and second fundamental forms, $a_{\alpha\beta}$, $b_{\alpha\beta}$, respectively [3, 10]

$$\sigma^{\alpha\beta} = \rho(\frac{\partial F(\rho, H, K; x^{\alpha})}{\partial a_{\alpha\beta}} + \frac{\partial F(\rho, H, K; x^{\alpha})}{\partial a_{\beta\alpha}}), \tag{5}$$

$$M^{\alpha\beta} = \frac{\rho}{2}(\frac{\partial F(\rho, H, K; x^{\alpha})}{\partial b_{\alpha\beta}} + \frac{\partial F(\rho, H, K; x^{\alpha})}{\partial b_{\beta\alpha}}), \tag{6}$$

where ρ is the surface mass density. H and K are mean and Gaussian curvatures given by

$$H = \frac{1}{2}a^{\alpha\beta}b_{\alpha\beta}, \quad K = \frac{1}{2}\varepsilon^{\alpha\beta}\varepsilon^{\lambda\mu}b_{\alpha\lambda}b_{\beta\mu}. \tag{7}$$

Here $(a^{\alpha\beta}) = (a_{\alpha\beta})$ is the dual metric and $\varepsilon^{\alpha\beta}$ is the permutation tensor defined by $\varepsilon^{12} = -\varepsilon^{21} = \frac{1}{\sqrt{a}}, \varepsilon^{11} = \varepsilon^{22} = 0$.

A reasonable assumption to make is that the membrane tubule has a fixed area. We introduce an area incompressibility ($J = 1$) constraint using a general form of free energy density per unit mass given as

$$F(\rho, H, K; x^\alpha) = \tilde{F}(H, K; x^\alpha) - \frac{\gamma(x^\alpha, t)}{\rho}. \tag{8}$$

Here $\gamma(x^\alpha, t)$ is a Lagrange multiplier field required to impose invariance of ρ on the whole of the surface (see [10] for full derivation). Substituting $W = \rho\tilde{F}$ into Eq. 8 we get

$$\sigma^{\alpha\beta} = (\lambda + W)a^{\alpha\beta} - (2HW_H + 2\kappa W_K)a^{\alpha\beta} + W_H\tilde{b}^{\alpha\beta}, \tag{9}$$

$$M^{\alpha\beta} = \frac{1}{2}W_H a^{\alpha\beta} + W_K\tilde{b}^{\alpha\beta}, \tag{10}$$

where

$$\lambda = -(\gamma + W). \tag{11}$$

Combining Eqs. 10, 4, and 3 into Eq. 1 gives the equations in normal and tangential equations as

$$\begin{aligned} p + \mathbf{f}\cdot\mathbf{n} = \Delta\frac{1}{2}W_H + (W_K)_{;\alpha\beta}\tilde{b}^{\alpha\beta} + W_H(2H^2 - K) \\ +2H(KW_K - W) - 2\lambda H, \end{aligned} \tag{12}$$

and

$$\begin{aligned} N^{\beta\alpha}_{;\alpha} - S^\alpha b^\beta_\alpha &= -(\gamma_{,\alpha} + W_K k_{,\alpha} + W_H H_{,\alpha})a^{\beta\alpha} \\ &= (\frac{\partial W}{\partial x^\alpha_{|exp}} + \lambda_{,\alpha})a^{\beta\alpha} = \mathbf{f}\cdot\mathbf{a}_s. \end{aligned} \tag{13}$$

Here $\Delta(\cdot)$ is the surface Laplacian and $()_{|exp}$ denotes the explicit derivative respect to coordinate θ^α.

Axisymmetric model

Using the axisymmetric parametrization

$$\mathbf{r}(s,\theta) = r(s)\mathbf{e}_r(\theta) + z(s)\mathbf{k}. \tag{14}$$

we define ψ as the angle made by the tangent with respect to the horizontal (see Fig. 1). This gives $r'(s) = \cos(\psi)$, $z'(s) = \sin(\psi)$, which satisfies the identity $(r')^2 + (z')^2 = 1$. Using this, we define the normal to the surface as $\mathbf{n} = -\sin\psi\mathbf{e}_r(\theta) + \cos\psi\mathbf{k}$, the tangent to the surface in the direction of increasing arc length as $\mathbf{a}_s = \cos\psi\mathbf{e}_r(\theta) + \sin\psi\mathbf{k}$, and unit vector τ = $\mathbf{e}_\theta$ tangent to the boundary $\partial\omega$ in the direction of the surface of revolution. For more details, we refer the reader to [10, 11, 12].

The expressions for tangential (κ_ν), transverse (κ_τ) and twist (τ) curvatures are simplified as

$$\kappa_\nu = \psi^{'}, \quad \kappa_\tau = r^{-1}\sin\psi, \quad \tau = 0. \tag{15}$$

Further, we calculate the mean curvature (H) and Gaussian curvature (K) as

$$H = \frac{1}{2}(\kappa_\nu + \kappa_\tau) = \frac{1}{2}(\psi^{'} + r^{-1}\sin\psi), \quad K = \kappa_\tau\kappa_\nu = \frac{\psi^{'}\sin\psi}{r}. \tag{16}$$

We introduce a term $L = \frac{1}{2\kappa}r(W_H)'$ in order to write a system of first order differential equations governing the problem [11] as ,

$$\begin{aligned}
r' &= \cos\psi, \quad z' = \sin\psi, \\
r\psi' &= 2rH - \sin\psi, \quad rH' = L + rC', \\
\frac{L'}{r} &= \frac{p}{k} + \frac{\mathbf{f}\cdot\mathbf{n}}{\kappa} + 2H\left[(H-C)^2 + \frac{\lambda}{\kappa}\right] \\
&\quad - 2\left(H-C\right)\left[H^2 + \left(H - r^{-1}\sin\psi\right)^2\right], \\
\lambda' &= 2\kappa\left(H-C\right)C' - \mathbf{f}\cdot\mathbf{a_s}.
\end{aligned} \tag{17}$$

Eq. 17 is a function of the arc length (s). This can be rewritten in terms of membrane area (a) using

$$a(s) = 2\pi\int_0^s r(\xi)d\xi \quad \rightarrow \quad \frac{da}{ds} = 2\pi r. \tag{18}$$

We choose to non-dimensionalize our system of equations using a length scale R_0 and bending rigidity scale κ_0 as

$$\begin{gathered}\alpha = \frac{a}{2\pi R_0^2}, \quad x = \frac{r}{R_0}, \quad y = \frac{y}{R_0}, \quad h = HR_0, \quad c = CR_0, \quad l = LR_0, \\ \lambda^* = \frac{\lambda R_0^2}{\kappa_0}, \quad p^* = \frac{pR_0^3}{\kappa_0}, \quad f^* = \frac{fR_0^3}{\kappa_0}, \quad \kappa^* = \frac{\kappa}{\kappa_0},\end{gathered} \tag{19}$$

where R_0 is the radius of the flat patch of membrane in simulations of a membrane tubule (Fig. 2E), the radius of the hemisphere for simulations of the tubule cap (Fig. 2B), and the radius of the tube for simulations of the tube (Fig. 2C) and the base (Fig. 2D). κ_0 is the bending rigidity of the bare membrane.

Rewriting Eq. 17 using the dimensionless variables in Eq. 19, we get [11]

$$\begin{aligned} x\dot{x} &= \cos\psi, \quad x\dot{y} = \sin\psi, \\ x^2\dot{\psi} &= 2xh - \sin\psi, \quad x^2\dot{h} = l + x^2\dot{c}, \\ \dot{l} &= \frac{p^*}{\kappa^*} + \frac{\mathbf{f}^* \cdot \mathbf{n}}{\kappa^*} + 2h\left[(h-c)^2 + \frac{\lambda^*}{\kappa^*}\right] \\ &\quad - 2\left(h-c\right)\left[h^2 + \left(h - x^{-1}\sin\psi\right)^2\right], \\ \dot{\lambda^*} &= 2\kappa^*\left(h-c\right)\dot{c} - \frac{\mathbf{f}^* \cdot \mathbf{a_s}}{x}. \end{aligned} \tag{20}$$

We enforce a third boundary point for constriction simulations at the base (Fig. 2D) and the whole tube (Fig. 2E) by introducing an independent variable [13]

$$\zeta = \alpha_{bp}\frac{\alpha - \alpha_{bp}}{\alpha_{tot} - \alpha_{bp}}, \tag{21}$$

where α_{bp} is the non-dimensional area of the first 'phase' and α_{tot} is the total non-dimensional area of the membrane. α is the variable defining the non-dimensional area along the first 'phase' and ζ is the variable defining non-dimensional area along the second 'phase'. Like α in the first interval, ζ ranges from o to α_{bp} in the second interval. Thus we can redefine our system of equations (Eq. 20) for 2 phases as

$$
\begin{aligned}
x_1\frac{dx_1}{d\alpha} &= \cos\psi_1, \quad x_1\frac{dy_1}{d\alpha} = \sin\psi_1,\\
x_1^2\frac{d\psi_1}{d\alpha} &= 2x_1h_1 - \sin\psi_1, \quad x_1^2\frac{dh_1}{d\alpha} = l_1 + x_1^2\dot{c_1},\\
\frac{dl_1}{d\alpha} &= \frac{p^*}{\kappa^*} + \frac{\mathbf{f_1^*}\cdot\mathbf{n}}{\kappa^*} + 2h_1\left[(h_1-c)^2 + \frac{\lambda_1^*}{\kappa^*}\right]\\
&\quad - 2\left(h_1-c_1\right)\left[h_1^2 + \left(h_1 - x_1^{-1}\sin\psi_1\right)^2\right],\\
\frac{d\lambda_1^*}{d\alpha} &= 2\kappa^*\left(h_1-c_1\right)\dot{c_1} - \frac{\mathbf{f_1^*}\cdot\mathbf{a_s}}{x},\\
x_2\frac{dx_2}{d\zeta} &= (\frac{\alpha_{tot}-\alpha_{bp}}{\alpha_{bp}})\cos\psi_2, \quad x_2\frac{dy_2}{d\zeta} = (\frac{\alpha_{tot}-\alpha_{bp}}{\alpha_{bp}})\sin\psi_2,\\
x_2^2\frac{d\psi_2}{d\alpha} &= (\frac{\alpha_{tot}-\alpha_{bp}}{\alpha_{bp}})(2x_2h_2 - \sin\psi_2),\\
x_2^2\frac{dh_2}{d\zeta} &= (\frac{\alpha_{tot}-\alpha_{bp}}{\alpha_{bp}})(l_2 + x_2^2)\dot{c_2},\\
\frac{dl_2}{d\zeta} &= (\frac{\alpha_{tot}-\alpha_{bp}}{\alpha_{bp}})(\frac{p^*}{\kappa^*} + \frac{\mathbf{f_2^*}\cdot\mathbf{n}}{\kappa^*} + 2h_2\left[(h_2-c_2)^2 + \frac{\lambda_2^*}{\kappa^*}\right]\\
&\quad - 2\left(h_2-c_2\right)\left[h_2^2 + \left(h_2 - x_2^{-1}\sin\psi_2\right)^2\right]),\\
\frac{d\lambda_2^*}{d\zeta} &= (\frac{\alpha_{tot}-\alpha_{bp}}{\alpha_{bp}})(2\kappa^*\left(h_2-c_2\right)\dot{c_2} - \frac{\mathbf{f_2^*}\cdot\mathbf{a_s}}{x}),
\end{aligned}
\tag{22}
$$

where 1 and 2 are the two phases represented by non-dimensional areas α and ζ, both of which are defined in the interval [0 α_{bp}]. Applied forces are modeled as a smooth hyperbolic tangent function. For example, the axial force at the tip of the tubule and radial force at the interface are modeled as

$$
f_{axial} = f_{ax} \times (0.5(1 - \tanh(\mathrm{g} * (\alpha - \alpha_{\text{axial}}))))/\alpha_{\text{axial}}, \tag{23}
$$

$$
\begin{aligned}
f_{pinch} = f_p \times 0.5(&\tanh(g(\alpha - (\alpha_{bp} - \alpha_{\text{radial}})))\\
&-0.5\tanh(g(\alpha - \alpha_{bp}))),
\end{aligned}
\tag{24}
$$

where f_{axial} and f_{pinch} are the distribution of axial and radial forces per unit area along the non-dimensional membrane area α, f_{ax} and f_p are the magnitudes for force per unit area, and α_{axial} and α_{radial} are the corresponding non-dimensional areas of applied force in the axial and radial direction respectively. g is a constant that ensures a sharp but smooth transition. In our simulations, we use g = 20 [11].

Boundary conditions

Eq 22 can be solved given a set of boundary conditions. All the axisymmetric simulations in this study were performed using the MATLAB bvp4c toolbox [13]. A useful feature of this toolbox is the estimation of unknown

parameters by providing additional boundary conditions [13]. The MATLAB subroutines used in this work are available on Github [14].

- **Whole tubule**

The tubule pinching simulations in Fig. 2E were performed using the following set of boundary conditions

$$\begin{aligned} x_1(0) = 0, \quad x_1(\alpha_{bp}) = \mathbf{x_p}, \quad \psi_1(0) = 0, \quad \psi_2(\alpha_{bp}) = 0, \\ y_1(0) = \mathbf{y_p}, \quad y_2(\alpha_{bp}) = 0, \quad , \lambda_2(\alpha_{bp}) = \boldsymbol{\lambda_0}, \quad l_1(0) = 0, \\ x_1(\alpha_{bp}) = x_2(0), \quad y_1(\alpha_{bp}) = y_2(0), \quad \psi_1(\alpha_{bp}) = \psi_2(0), \\ h_1(\alpha_{bp}) = h_2(0), \quad l_1(\alpha_{bp}) = l_2(0), \quad \lambda_1(\alpha_{bp}) = \lambda_2(0). \end{aligned} \tag{25}$$

$\mathbf{x_p}$ and $\mathbf{y_p}$ are additional constraints for the radius at the interface and height of the tubule respectively. These additional constraints are used to estimate the axial force and pinching force required to obtain a solution to the system of equations in Eq. 22. $\boldsymbol{\lambda_0}$ is the boundary membrane tension. We note here that this now represents a system of 12 equations and 2 unknown parameters with 14 boundary conditions. The 2 unknown parameters are the axial and radial force. 6 of these boundary conditions are continuity conditions for every parameter at the interface (Eq. 25).

- **Base**

The half catenoid-like base pinching simulations in Fig. 2D were performed using the following set of boundary conditions

$$\begin{aligned} x_1(0) = \mathbf{x_0}, \quad x_1(\alpha_{bp}) = \mathbf{x_p}, \quad \psi_1(0) = \pi, \quad \psi_2(\alpha_{bp}) = \pi/2, \\ y_1(0) = 0, \quad , \lambda_1(0) = \boldsymbol{\lambda_0}, \quad l_2(\alpha_{bp}) = 0, \\ x_1(\alpha_{bp}) = x_2(0), \quad y_1(\alpha_{bp}) = y_2(0), \quad \psi_1(\alpha_{bp}) = \psi_2(0), \\ h_1(\alpha_{bp}) = h_2(0), \quad l_1(\alpha_{bp}) = l_2(0), \quad \lambda_1(\alpha_{bp}) = \lambda_2(0). \end{aligned} \tag{26}$$

$\mathbf{x_p}$ is the additional constraint for the radius at the interface. $\mathbf{x_0}$ is the radius at y = 0. The additional constraint is used to estimate the pinching force required to obtain a solution to the system of equations in Eq. 22. $\boldsymbol{\lambda_0}$ is the boundary membrane tension. We note here that this now represents a system of 12 equations and 1 unknown parameter with 13 boundary conditions.

- **Tube**

The cylinder/tube pinching simulations in Fig. 2C were performed by solving the system of equations in Eq. 20 for a single phase of membrane. The boundary conditions used were

$$\begin{aligned} l(0) = 0, \quad y(0) = 0, \quad y(\alpha) = Z_0/R_0, \quad \psi(0) = \pi/2, \\ x(\alpha) = 1, \quad x(0) = \mathbf{x_p}, \quad \psi(\alpha) = \pi/2, \end{aligned} \tag{27}$$

where α is the non-dimensional area of the tube, $\mathbf{x_p}$ is the additional constraint required for estimating the pinching force. This represents a system of 6 equations and 1 unknown parameter with 7 boundary conditions.

- **Cap**

The hemisphere/cap pinching simulations in figure 2B were performed by solving the system of equations in Eq. 20 for a single phase of membrane. The boundary conditions used were

$$\begin{aligned} l(0) = 0, \quad y(0) = 0, \quad l(\alpha) = 0, \quad \psi(0) = \pi/2, \\ x(\alpha) = 0, \quad x(0) = \mathbf{x_p}, \quad \psi(\alpha) = \pi, \end{aligned} \tag{28}$$

where $\mathbf{x_p}$ is the additional constraint required for estimating the pinching force. This represents a system of 6 equations and 1 unknown parameter with 7 boundary conditions.

3D model

Thin shell formulation

Considering the classical Helfrich formulation for biological membranes, the strain energy density of a membrane in the current configuration is given by:

$$W = k_B(H - H_0)^2 + k_G\kappa \tag{29}$$

where k_B and k_G are the bending modulus and the Gaussian modulus of the membrane, H is the mean curvature, κ is the Gaussian curvature and H_0 represents the instantaneous curvature induced in the membrane.

To enforce area-incompressibility, we consider the following Lagrange multiplier formulation:

$$W_{LM} = J(k_B(H - H_0)^2 + k_G\kappa) + q(J - 1) \tag{30}$$

where q is the point value of the Lagrange multiplier field, and J is the surface stretch (ratio of area in the current configuration to the area in the reference configuration).

The governing equation for quasi-static mechanical equilibrium in 3D simulations is obtained by minimizing the Helfrich energy functional following standard variational arguments, and is given by [5]:

$$\int_{\partial\Omega} \frac{1}{2}\delta a_{ij}\sigma^{ij}\, da + \int_{\partial\Omega} \delta b_{ij} M^{ij}\, da - \int_{\partial\Omega_{\text{collar}}} \delta\boldsymbol{x}\cdot\boldsymbol{p}\, da - \int_{\Gamma} \delta\boldsymbol{x}\cdot\boldsymbol{t}\, ds = 0 \tag{31}$$

where $\partial\Omega$ is the membrane surface and Γ is the membrane boundary on which surface tractions can be applied, as shown in Figure 1B. δa_{ij} and δb_{ij} are variations of the components of the metric tensor and the curvature tensor, respectively. σ^{ij} are the components of the stress tensor, M^{ij} are components of the moment tensor, $\boldsymbol{p}$ is the pressure applied along a collar on the membrane surface (to cause constriction), and $\boldsymbol{t}$ is the surface traction.

For a hyperelastic material model, we can express the stress and moment components in terms of the strain energy density as [15]:

$$\sigma^{ij} = \frac{2}{J}\frac{\partial W}{\partial a_{ij}} \tag{32}$$

$$M^{ij} = \frac{1}{J}\frac{\partial W}{\partial b_{ij}} \tag{33}$$

For the Helfrich type strain energy density, these take the form:

$$\sigma^{ij} = (k_B(H-H_0)^2 - k_G\kappa)a^{ij} - 2k_B(H-H_0)b^{ij} \tag{34}$$

$$M^{ij} = (k_B(H-H_0) + 2k_G H)a^{ij} - k_G b^{ij} \tag{35}$$

Computational implementation

We solve the governing equation given by Eq.31 using a Isogeometric Analysis (IGA) based numerical framework for solving problems of membrane mechanics developed as part of this work. A companion manuscript (in preparation by the authors) describes the details of the mathematical methods and the numerical formulation. The computational implementation, along with the source code for solving the boundary value problems listed below, is available as a public code repository on GitHub [16].

List of 3D simulations

For each of the 3D simulations, we solve the governing equation given by Eq.31 using a force control or displacement control approach, with the relevant displacement, angle and traction boundary conditions. The displacement boundary conditions are applied on the components of the displacement vector, $\boldsymbol{u}$, that is defined as

the change in position of a point on the membrane between its current and reference configuration ($\boldsymbol{u}(\xi_1, \xi_2) = \mathbf{x}(\xi_1, \xi_2) - \mathbf{X}(\xi_1, \xi_2)$). The angle boundary conditions, where needed, are enforced through the weak formulation using a penalty approach and result in the normal vector ($\mathbf{n}$) at the boundaries to align along the preferred direction. In all the simulations, we have two boundaries, and these are identified as the inner boundary (Γ_{I}) and the outer boundary (Γ_{O}) as indicated in the schematic in Figure 1B. The specific numerical simulations in this work using the 3D model are described below.

- **Tube pulling**

  The tube pulling simulation shown in Figure S1(A) considers a reference circular plate geometry with an outer radius of 20 nm, and an inner radius of 0.2 nm. The boundary value problem is solved as a force control problem with a traction on the inner boundary (Γ_{I}). The displacement and traction boundary conditions are as follows:

$$
\begin{aligned}
t_y &= h \quad \text{on} \quad \Gamma_{\mathrm{I}} \\
u_x &= 0 \quad \& \quad u_z = 0 \quad \text{on} \quad \Gamma_{\mathrm{I}} \\
u_y &= 0 \quad \text{on} \quad \Gamma_{\mathrm{O}}
\end{aligned}
$$

  See Movie M12 in the supplementary information for the evolution of the membrane deformation.

- **Whole tubule**

  The whole tubule simulations shown in Figure 4 consider pinching at three different locations, identified as the cap, tube and base locations (Figure 2A). For the tubule geometry, shown in Figure 2A, the tubule radius is 20 nm and height is 100 nm. The inner boundary (Γ_{I}) at the top of the tubule has a radius of 0.2 nm and the outer boundary (Γ_{O}) at the base of the tubule has a radius of 40 nm. The boundary value problem is solved as a force control problem with pressure applied on a collar (Ω_{collar}) located at the cap, tube or base location. In addition, the displacement boundary conditions are as follows:

$$
\begin{aligned}
u_x &= 0 \quad \text{on} \quad \Gamma_{\mathrm{I}} \\
u_y &= 0 \quad \text{on} \quad \Gamma_{\mathrm{I}} \\
u_z &= 0 \quad \text{on} \quad \Gamma_{\mathrm{I}}
\end{aligned}
$$

  See Movies M1-M3 in the supplementary information for the evolution of the constriction process for the cap, tube and base locations.

- **Base**

  The constriction simulation shown in Figure 5 considers pinching at the base location. The tube geometry considered has a radius of 20 nm, and a height of 80 nm. The tube boundary on the top is identified as

the inner boundary (Γ_{I}) and the tube boundary at the bottom is identified as the outer boundary (Γ_{O}). The boundary value problem is solved as a force control problem with pressure applied on a collar (Ω_{collar}) located at the base location. In addition, the displacement boundary conditions are as follows:

$$u_x = 0 \quad \text{on} \quad \Gamma_{\mathrm{I}}$$
$$u_y = 0 \quad \text{on} \quad \Gamma_{\mathrm{I}}$$
$$u_z = 0 \quad \text{on} \quad \Gamma_{\mathrm{I}}$$

See Movie M3 in the supplementary information for the evolution of the constriction process for the base location.

- **Cap**

The constriction simulation shown in Figure S3 considers pinching at the cap location. The cap geometry is a hemisphere with a radius of 20 nm. The cap boundary on the top, with a small radius of 1 nm, is identified as the inner boundary (Γ_{I}) and the cap boundary at the bottom is identified as the outer boundary (Γ_{O}). This boundary value problem is solved as a displacement control problem, as the force control problem is numerically unstable due to the rigid body modes induced under the displacement boundary conditions considered. As this problem is solved as a displacement control problem, this enforces axisymmetry of the pinching profile. The displacement boundary conditions are as follows:

$$u_x = g \quad \text{on} \quad \Gamma_{\mathrm{O}}$$
$$u_y = 0 \quad \text{on} \quad \Gamma_{\mathrm{O}}$$
$$u_z = g \quad \text{on} \quad \Gamma_{\mathrm{O}}$$

See Movie M13 in the supplementary information for the evolution of the constriction process for the cap location.

- **Tube**

The constriction simulation shown in Figure S4 considers pinching at the tube location. The tube geometry is a cylinder with a radius of 20 nm. The tube boundary on the top is identified as the inner boundary (Γ_{I}) and the boundary at the bottom is identified as the outer boundary (Γ_{O}). This boundary value problem is solved as a displacement control problem. Like in the case of the cap simulation, as this problem is solved as a displacement control problem, this enforces axisymmetry of the pinching profile. The displacement

boundary conditions are as follows:

$$u_x = g \quad \text{on} \quad \Gamma_{\mathrm{O}}$$
$$u_z = g \quad \text{on} \quad \Gamma_{\mathrm{O}}$$
$$u_y = 0 \quad \text{on} \quad \Gamma_{\mathrm{I}}$$

See Movie M14 in the supplementary information for the evolution of the constriction process with displacement control for the tube location.

We also solve a force control equivalent of this problem, and this is shown in Figure S5. This case is discussed below in the simulation of the helical force collar at the tube location with a zero helical pitch. See Movie M15 in the supplementary information for the evolution of the constriction process with force control for the tube location.

- **Helical force collar at the tube location**

  The constriction simulation shown in Figure 6 considers pinching at the tube location due to helical collar. In Figure 6A we consider a single helical ring, and in Figure 6G we consider three helical rings. The tube geometry considered for the single helical ring case has a radius of 20 nm, and a height of 40 nm. The tube geometry considered for the three helical rings case has a radius of 20 nm, and a height of 200 nm. For both cases, the tube boundary on the top is identified as the inner boundary (Γ_{I}) and the tube boundary at the bottom is identified as the outer boundary (Γ_{O}). The boundary value problem is solved as a force control problem with pressure applied on a helical collar (Ω_{collar}) located at the tube location. In addition, the displacement boundary conditions are as follows:

$$u_x = 0 \quad \text{on} \quad \Gamma_{\mathrm{I}}$$
$$u_y = 0 \quad \text{on} \quad \Gamma_{\mathrm{I}}$$
$$u_z = 0 \quad \text{on} \quad \Gamma_{\mathrm{I}}$$
$$u_x = 0 \quad \text{on} \quad \Gamma_{\mathrm{O}}$$
$$u_y = 0 \quad \text{on} \quad \Gamma_{\mathrm{O}}$$
$$u_z = 0 \quad \text{on} \quad \Gamma_{\mathrm{O}}$$

  See Movies M4-M6 in the supplementary information for the evolution of the constriction process due to a helical force collar at the tube location with a non-dimensional pitch of zero, two and four, respectively, and movie M7 for the corresponding evolution of the constriction process due to a force collar with three helical rings.

- **Helical force collar at the base location**

  The constriction simulation shown in Figure 7 considers pinching at the base location due to helical collar. In Figure 7A we consider a single helical ring, and in Figure 7G we consider three helical rings. The tube geometry considered for the single helical ring case has a radius of 20 nm, and a height of 40 nm. The tube geometry considered for the three helical rings case has a radius of 20 nm, and a height of 200 nm. For both cases, the tube boundary on the top is identified as the inner boundary (Γ_{I}) and the tube boundary at the bottom is identified as the outer boundary (Γ_{O}). The boundary value problem is solved as a force control problem with pressure applied on a helical collar (Ω_{collar}) located at the base location. In addition, the displacement boundary conditions are as follows:

$$u_x = 0 \quad \text{on} \quad \Gamma_{\mathrm{I}}$$
$$u_y = 0 \quad \text{on} \quad \Gamma_{\mathrm{I}}$$
$$u_z = 0 \quad \text{on} \quad \Gamma_{\mathrm{I}}$$

  See Movies M8-M10 in the supplementary information for the evolution of the constriction process due to a helical force collar at the base location with a non-dimensional pitch of zero, two and four, respectively, and movie M11 for the corresponding evolution of the constriction process due to a force collar with three helical rings.

Analytical solution for tube pulling simulation

The equilibrium values of R_0 and f_0 for a membrane tube are defined as

$$R_0 = \sqrt{\kappa/(2\sigma)}, \tag{36}$$
$$f_0 = 2\pi\sqrt{(2\sigma\kappa)}, \tag{37}$$

where κ is the bending rigidity, σ is the membrane tension. For bending rigidity of 20 pN·nm and membrane tension 0.1 pN/nm, we get

$$f_0 = 12.5664 \text{ pN}, \tag{38}$$

which is the equilibrium value of force obtained in Fig. S1.

List of movies

- Movie M1: Evolution of the constriction process for the cap location for the whole tubule geometry.
- Movie M2: Evolution of the constriction process for the tube location for the whole tubule geometry.
- Movie M3: Evolution of the constriction process for the base location for the whole tubule geometry.
- Movie M4: Evolution of the constriction process due to a single helical force collar at the tube location with a non-dimensional pitch of zero.
- Movie M5: Evolution of the constriction process due to a single helical force collar at the tube location with a non-dimensional pitch of two.
- Movie M6: Evolution of the constriction process due to a single helical force collar at the tube location with a non-dimensional pitch of four.
- Movie M7: Evolution of the constriction process due to a force collar with three helical rings at the tube location.
- Movie M8: Evolution of the constriction process due to a single helical force collar at the base location with a non-dimensional pitch of zero.
- Movie M9: Evolution of the constriction process due to a single helical force collar at the base location with a non-dimensional pitch of two.
- Movie M10: Evolution of the constriction process due to a single helical force collar at the base location with a non-dimensional pitch of four.
- Movie M11: Evolution of the constriction process due to a force collar with three helical rings at the base location.
- Movie M12: Evolution of membrane deformation for pulling of a tubule from a flat membrane.
- Movie M13: Evolution of a axisymmetric constriction profile due to a displacement control approach of constriction at the cap location.
- Movie M14: Evolution of a axisymmetric constriction profile due to a displacement control approach of constriction at the tube location.
- Movie M15: Evolution of a non-axisymmetric constriction profile due to a force control approach of constriction at the tube location.

References

[1] Wolfgang Helfrich. Elastic properties of lipid bilayers: theory and possible experiments. Zeitschrift für Naturforschung C, 28(11-12):693–703, 1973.

[2] EA Evans and R Skalak. Mechanics and thermodynamics of biomembranes: part 1. CRC critical reviews in bioengineering, 3(3):181–330, 1979.

[3] Padmini Rangamani, Ashutosh Agrawal, Kranthi K Mandadapu, George Oster, and David J Steigmann. Interaction between surface shape and intra-surface viscous flow on lipid membranes. Biomechanics and modeling in mechanobiology, 12(4):833–845, 2013.

[4] Mijo Simunovic, Jean-Baptiste Manneville, Henri-François Renard, Emma Evergren, Krishnan Raghunathan, Dhiraj Bhatia, Anne K Kenworthy, Gregory A Voth, Jacques Prost, Harvey T McMahon, et al. Friction mediates scission of tubular membranes scaffolded by bar proteins. Cell, 170(1):172–184, 2017.

[5] Roger Sauer, Thang Duong, Kranthi Mandadapu, and David Steigmann. A stabilized finite element formulation for liquid shells and its application to lipid bilayers. Journal of Computational Physics, 330:436–466, 2017.

[6] Drazen Raucher and Michael P Sheetz. Characteristics of a membrane reservoir buffering membrane tension. Biophysical journal, 77(4):1992–2002, 1999.

[7] Jon Mulholland, Daphne Preuss, Anne Moon, Amie Wong, David Drubin, and David Botstein. Ultrastructure of the yeast actin cytoskeleton and its association with the plasma membrane. The Journal of cell biology, 125(2):381–391, 1994.

[8] Nikhil Walani, Jennifer Torres, and Ashutosh Agrawal. Endocytic proteins drive vesicle growth via instability in high membrane tension environment. Proceedings of the National Academy of Sciences, 112(12):E1423–E1432, 2015.

[9] Michael M Kozlov. Fission of biological membranes: interplay between dynamin and lipids. Traffic, 2(1):51–65, 2001.

[10] DJ Steigmann. Fluid films with curvature elasticity. Archive for Rational Mechanics and Analysis, 150(2):127–152, 1999.

[11] Julian E Hassinger, George Oster, David G Drubin, and Padmini Rangamani. Design principles for robust vesiculation in clathrin-mediated endocytosis. Proceedings of the National Academy of Sciences, 114(7):E1118–E1127, 2017.

[12] Padmini Rangamani, Kranthi K Mandadap, and George Oster. Protein-induced membrane curvature alters local membrane tension. Biophysical journal, 107(3):751–762, 2014.

[13] Lawrence F Shampine, Jacek Kierzenka, and Mark W Reichelt. Solving boundary value problems for ordinary differential equations in matlab with bvp4c. Tutorial notes, 2000:1–27, 2000.

[14] R. Vasan. Membrane-neck-formation. https://github.com/ritvikvasan/Membrane-neck-formation, 2019.

[15] Roger A Sauer and Thang X Duong. On the theoretical foundations of thin solid and liquid shells. Mathematics and Mechanics of Solids, 22(3):343–371, 2017.

[16] S. Rudraraju. Code repository for kirchhoff-love shell kinematics and applications to mechanics of biological membranes. https://github.com/cmmg/biologicalMembraneMechanics, 2019.

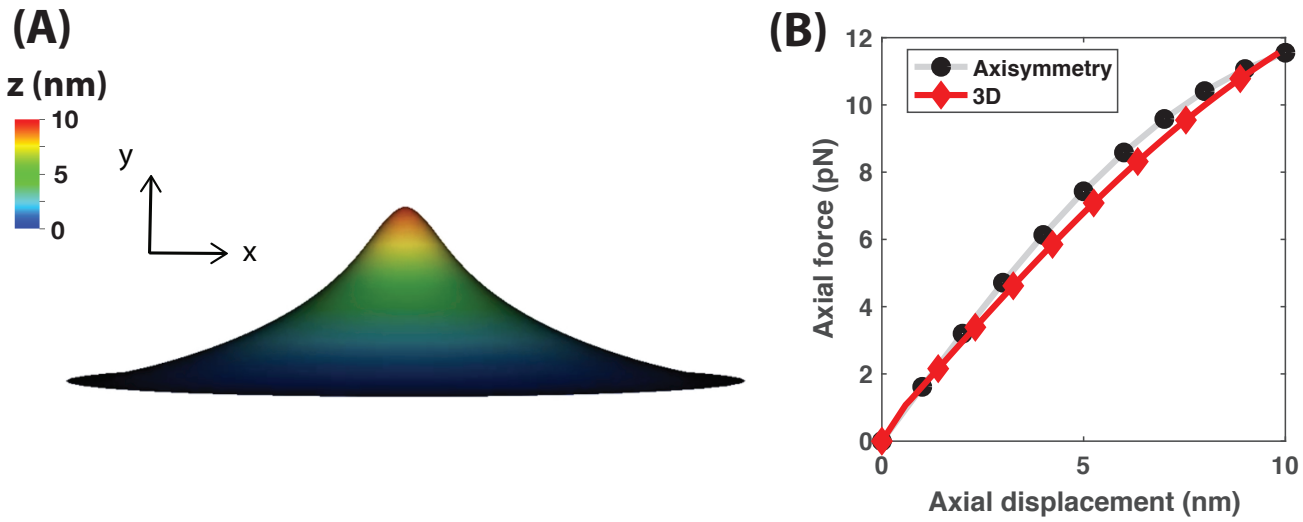

Figure S1: Comparison of the axial force required to deform a flat membrane patch up to a height of 10 nm. Bending rigidity is 20 pN·nm and membrane tension is 0.1 pN/nm. The results obtained from the axisymmetric model and the 3D framework are compared. The analytical solution for the equilibrium value of force is 12.5664 pN. (A) Membrane shape at a deformation of 10 nm. Colorbar indicates the height (nm). (B) Axial force vs height of membrane in axisymmetry and 3D. See Movie M12 in the supplementary information for the evolution of the membrane deformation.

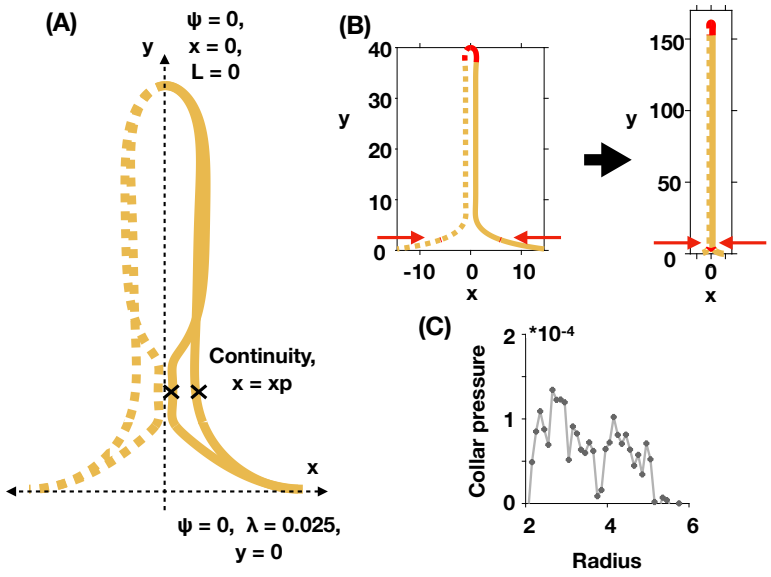

Figure S2: No snap-through instability is observed for constriction at the base of a tubule without the fixed height boundary condition. Membrane tension is 0.2 pN/nm, bending rigidity is 320 pN·nm. (A) Schematic depicting the boundary conditions used. The difference with the B.Cs in Eq. 25 is that the height is no longer constrained. This implies that the axial force is fixed. Thus, this simulation represents a system of 12 equations with 1 unknown parameter and 13 boundary conditions (Eq. 22). (B) Initial and final membrane shapes obtained for constriction at the base of the tubule. (C) Collar pressure vs radius at the break point. Pressure is negligible (order of magnitude is 10^{-4}.)

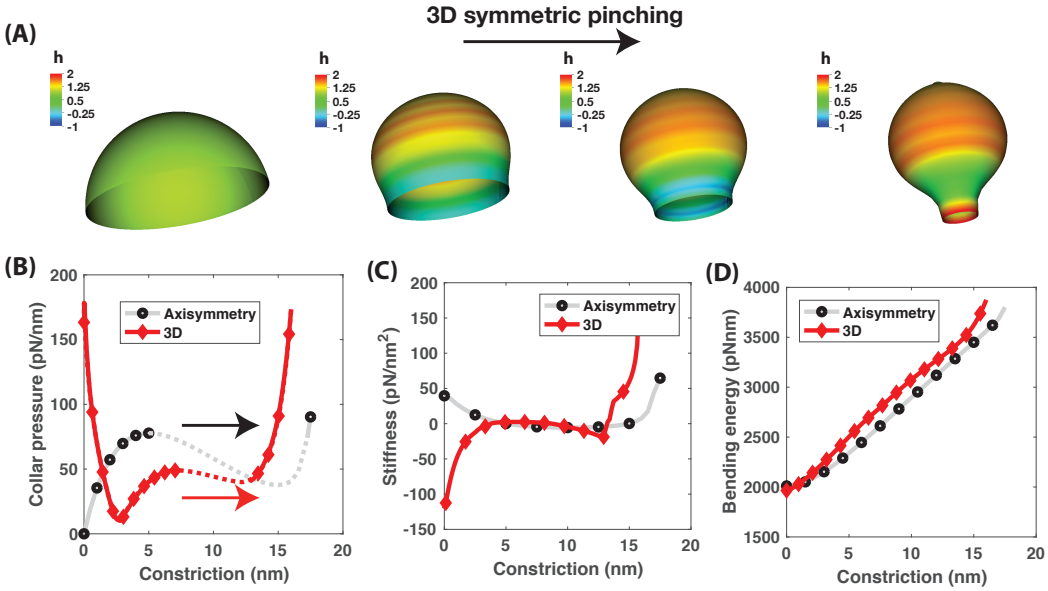

Figure S3: Comparison of collar pressure, stiffness and bending energy during constriction of a membrane cap using the axisymmetric and 3D framework. Axisymmetry is enforced in the 3D simulation by solving as a displacement control problem. Boundary conditions used are shown in Fig. 1, case 1. Bending rigidity is 320 pN/nm, Radius is 20 nm. (A) Membrane shapes during constriction of spherical membrane in 3D. Colorbar is the normalized mean curvature. (B) Collar pressure vs constriction in 3D and axisymmetry. (C) Stiffness vs constriction in 3D and in axisymmetry. (D) Bending energy vs constriction in 3D and axisymmetry. See Movie M13 in the supplementary information for the evolution of the constriction process.

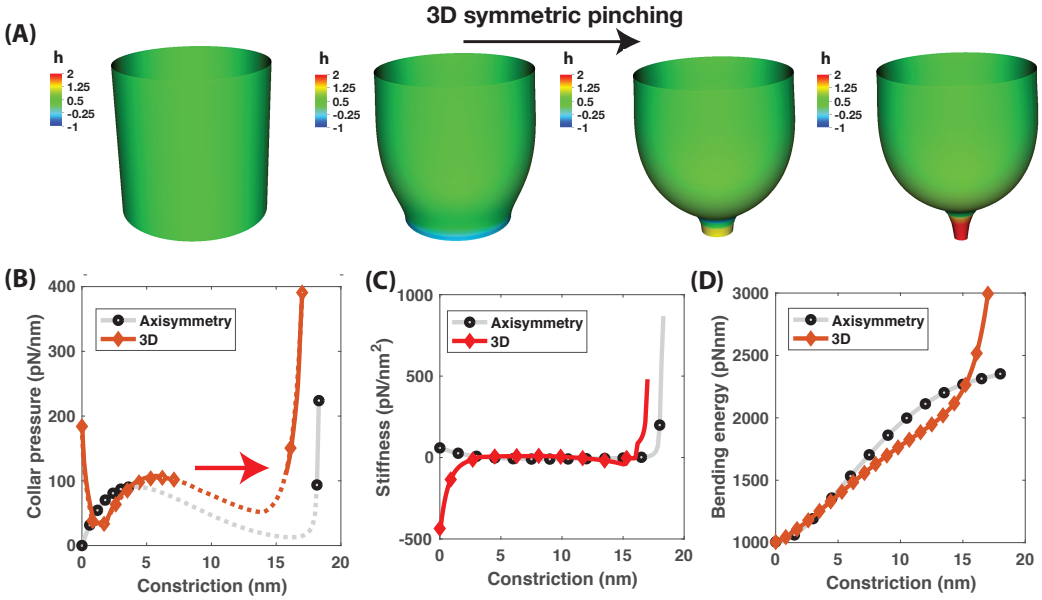

Figure S4: Comparison of collar pressure, stiffness and bending energy during constriction of a membrane cylinder using the axisymmetric and 3D framework. Axisymmetry is enforced in the 3D simulation by solving as a displacement control problem. Boundary conditions used are those shown in Fig. 1, case 2. Bending rigidity is 320 pN · nm, length scale R_0 is 20 nm. (A) Membrane shapes during constriction of cylindrical membrane in 3D. Colorbar is the normalized mean curvature. (B) Collar pressure vs constriction in 3D and axisymmetry. (C) Stiffness vs constriction in 3D and in axisymmetry. (D) Bending energy vs constriction in 3D and axisymmetry. See Movie M14 in the supplementary information for the evolution of the constriction process.

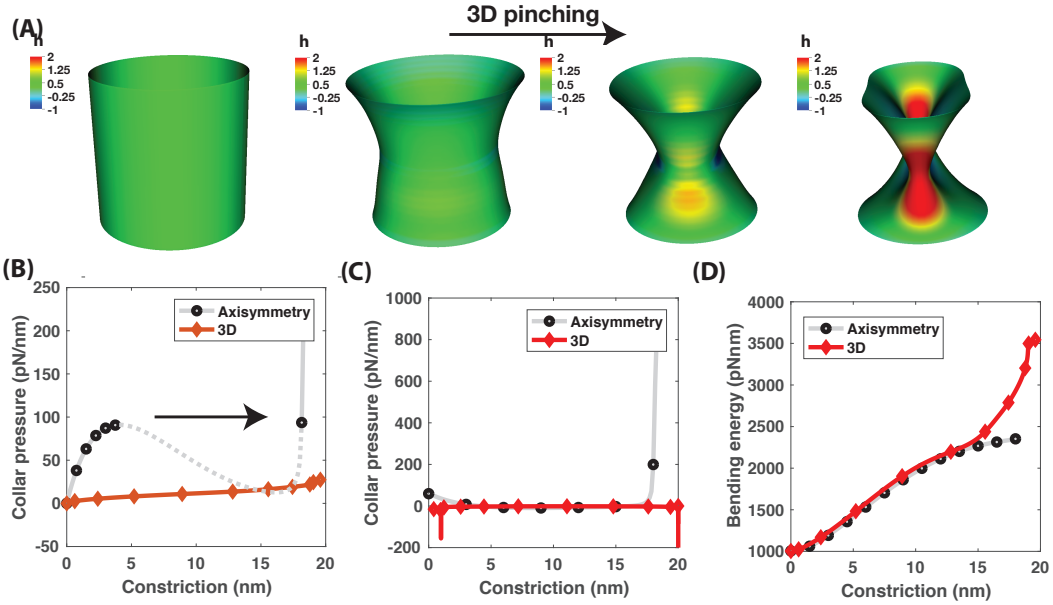

Figure S5: Comparison of collar pressure, stiffness and bending energy during constriction of a membrane cylinder using the axisymmetric and 3D framework. Bending rigidity is 320 pN/nm, Radius is 20 nm. (A) Membrane shapes during constriction of cylindrical membrane in 3D. Colorbar is the normalized mean curvature. (B) Collar pressure vs constriction in 3D and axisymmetry. (C) Stiffness vs constriction in 3D and in axisymmetry. (D) Bending energy constriction in 3D and axisymmetry. See Movie M15 in the supplementary information for the evolution of the constriction process.

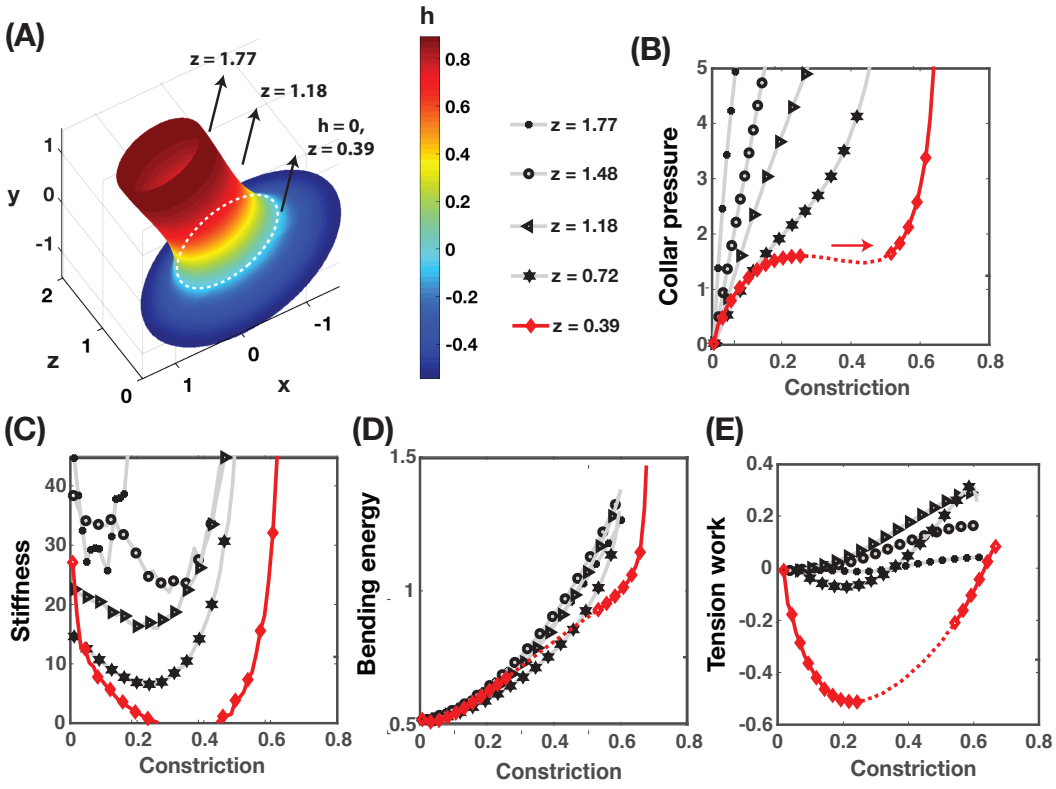

Figure S6: The snap-through instability for constriction at the base is regulated by a variation in local tension. Membrane tension at the boundary is 0.2 pN/nm, bending rigidity is 320 pNnm, Radius is 20 nm, area of applied force is 1/200th of the membrane area. z is the non-dimensional height at a given location along the membrane from the bottom. Shown are the (A) Mean curvature distribution (non-dimensional) and the location of the local minimal surface (dotted line at y = 0.39) where the mean curvature vanishes ($h = 0$), (B) Collar pressure, (C) Tubule stiffness to pinching, (D) Bending energy and (E) Tension work as a function of the constriction.